ORIGINAL RESEARCH PAPER

Fuel Cells DOI: 10.1002/fuce.201400071

Electrochemical Performance of $Nd_{1.95}NiO_{4+\delta}$ Cathode supported Microtubular Solid Oxide Fuel Cells

M. A. Laguna-Bercero[1]*, H. Luebbe[2,3], J. Silva[1], J. Van herle[2]

[1] Instituto de Ciencia de Materiales de Aragón (ICMA), CSIC-Universidad de Zaragoza, C/ Pedro Cerbuna 12, E-50009, Spain
[2] Ecole Polytechnique Fédérale de Lausanne, STI-IGM, Industrial Energy Systems Laboratory (LENI), Station 9, CH-1015 Lausanne, Switzerland
[3] Present address: ASULAB, Rue des Sors 3, CH-2074 MARIN, Switzerland

Received April 25, 2014; accepted October 04, 2014; published online October 28, 2014

Abstract

$Nd_{1.95}NiO_{4+\delta}$ (NNO) cathode supported microtubular cells were fabricated and characterized. This material presents superior oxygen transport properties in comparison with other commonly used cathode materials. The supporting tubes were fabricated by cold isostatic pressing (CIP) using NNO powders and corn starch as pore former. The electrolyte (GDC, gadolinia doped ceria based) was deposited by wet powder spraying (WPS) on top of pre-sintered tubes and then co-sintered. Finally, a NiO/GDC suspension was dip-coated and sintered as the anode. Optimization of the cell fabrication process is shown. Power densities at 750 °C of ~40 mWcm^{-2} at 0.5V were achieved. These results are the first electrochemical measurements reported using NNO cathode-supported microtubular cells. Further developments of the fabrication process are needed for this type of cells in order to compete with the standard microtubular solid oxide fuel cells (SOFC).

Keywords: Cathode-supported, K_2NiF_4-type structure, Microtubular, $Nd_2NiO_{4+\delta}$, SOFC

1 Introduction

Microtubular solid oxide fuel cells (mT-SOFC) have attracted interest in recent years [1–3]. In order to increase the variety of applications for SOFCs such as auxiliary power units (APU) for automobile and power sources for portable devices, it will be crucial to develop highly efficient small cell stacks which are robust for rapid temperature transient operation. So far, SOFC tubular designs were reported to be robust under thermal stress caused by a heating cycle [4]. Decreasing the tubular cell diameter is expected to further improve the mechanical properties as well as the volumetric power density of the stacks. In addition, microtubular SOFCs accommodate repeated and fast heat and electrical load cycling [4, 5]. They have also been proposed as microtubular solid oxide electrolysers (SOEC) for hydrogen production [6, 7].

The first generation of microtubular SOFC was reported by Kendall and Palin [5] and Kilbride [8] using YSZ (yttria stabilized zirconia) electrolyte supports produced by extrusion techniques, nickel-zirconia cermet for the anode and lanthanum strontium manganite (LSM) as the cathode. Current designs, i.e. second generation microtubular SOFC, focus on electrode-supported cells, as for the planar configuration. Choosing the anode as support is the preferred configuration, as widely studied by different research groups in the literature [9–14]. However, research on cathode supported cells is also of interest as they present some advantages in comparison with anode supported cells. The main advantage is an increased tolerance to volume contraction/expansion resulting from the accidental anode redox cycles, as in the cathode supported configuration the anode is a thin layer. In addition, when operating on hydrocarbon fuels with low steam-to-carbon ratio, a relatively thin anode would also prevent it from carbon deposition. Cathode supported microtubular cells have been investigated to much more limited extent in the literature, in part due to the chemical reactivity between cathode and electrolyte during the high temperature co-sintering step of the fabrication process. Liu *et al.* [15] reported cathode supported microtubular cells based on LSCF (lanthanum strontium cobalt ferrite)-GDC (gadolinia doped ceria) cathode supports, achieving power densities of about 160 mW cm^{-2} at 600 °C. Cathode supported cells based on LSM were proposed by Zhao *et al.* [16] with power densities of 157 mW cm^{-2} at 750 °C and 358 mW cm^{-2} at 850 °C. Yamaguchi *et al.* [17, 18] studied

[*] *Corresponding author, malaguna@unizar.es*

LSM cathode supported microtubular cells using ScSZ (scandia-stabilized zirconia) as the electrolyte, an LSM-GDC activation layer between the support and the electrolyte and a NiO/GDC anode layer. Although they found signs of reactivity between GDC and ScSZ, they achieved power densities of 453 mW cm^{-2} at 750 °C.

An alternative for the standard SOFC perovskite cathodes are the lanthanide nickelates (Ln = La, Nd, Pr), which have received considerable attention as materials for both solid oxide fuel cell (SOFC) electrodes and oxygen separation membranes [19–22]. These materials adopt a K_2NiF_4-type structure consisting of alternate $LnNiO_3$ perovskite layers and LnO rock-salt layers with excess oxygen ions occupying interstitial sites between the LnO layers. They present flexible oxygen stoichiometry, leading to fast oxygen ion diffusion through bulk materials as well as rapid surface exchange kinetics. For implementation of these materials in devices, their phase stability is of great importance at temperatures up to 1000 °C and over a wide pO_2 range. The main drawback of these nickelate phases is their reactivity with standard YSZ or GDC electrolytes, as reported for example by Philippeau *et al.* [23]. It was recently reported that infiltration of nickelate salt precursors followed by calcination avoids high temperature sintering of the nickelate phase with the electrolyte and as a consequence, prevents their reaction [24]. Recently, Luebbe *et al.* reported for the first time the fabrication of microtubular SOFCs using neodymium nickelate ($Nd_{1.95}NiO_{4+\delta}$, NNO) as the cathode support [25, 26].

In the present paper, fabrication and characterization of NNO cathode supported microtubular SOFCs including electrochemical results, using GDC as the electrolyte and NiO-GDC as the anode, will be reported.

2 Experimental

2.1 Cell Fabrication

$Nd_{1.95}NiO_{4+\delta}$ powders (Marion Technologies, France) were used for the fabrication of the supporting tubes. A Si-amount of about 1 at% is present as an endogenous impurity in the NNO powder. NNO powders were mixed with corn-starch (pore former) and polyvinyl alcohol (PVA) as binder. NNO tubes (Figure 1) were fabricated by cold isostatic pressing (CIP) at 200 MPa and presintered at 900 °C. GDC powder containing 2%wt cobalt-doping (Fuel Cell Materials, US) was deposited by wet powder spraying (WPS) using ethanol as liquid vehicle, for the electrolyte layer. In order to match the sintering of both NNO cathode and GDC electrolyte, dilatometric studies were performed. For this purpose, two cylindrical samples (isostatically pressed) of NNO and GDC, respectively, were heated up to 1400 °C (scan rate 2 °C/min) in a thermomechanical analyser (Setaram, SETSYS 200, France). As shown in Figure 2, NNO reached maximum contraction (~13%) at around 1370 °C, whereas the GDC electrolyte reached the maximum (~8%) at only 900 °C. As the sintering behavior of both phases differs considerably, it was not easy to find appropriate cosintering conditions. Moreover, we have tried to reduce the cosintering temperature (in the range of 1150 to 1250 °C) in order to limit reaction between the phases. However, the contraction of the NNO cathode was insufficient at these temperatures, producing cracking of the GDC electrolyte, as demonstrated in Figure 1 (c). Appropriate conditions were finally determined, as evidenced from Figure 1 (b), when the NNO electrode-GDC electrolyte was co-sintered at 1300 °C for 2 hours. NiO/GDC (50%-50%wt) was used as the anode composition, and was deposited by dip-coating and subsequently sintered at 1250 °C during 1.5 hours.

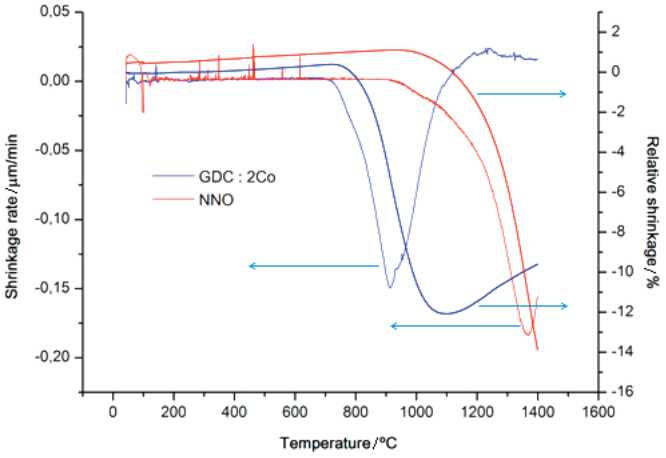

Fig. 2 Dilatometric studies for the NNO support and the GDC:2Co electrolyte.

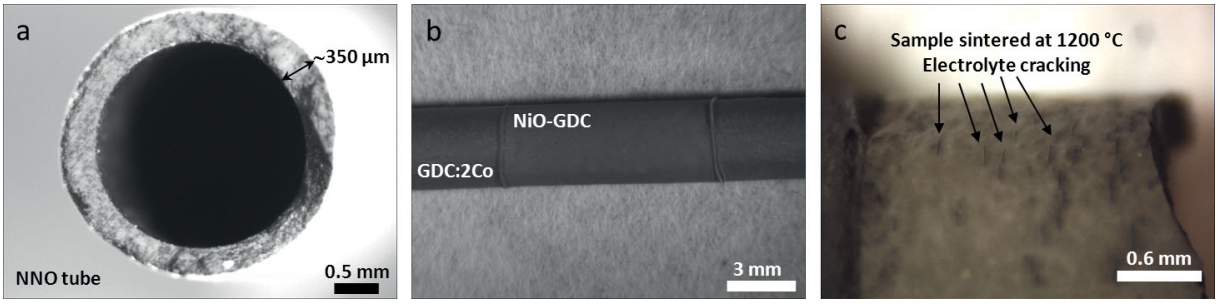

Fig. 1 (a) Cross- section of the microtubular NNO cathode support; (b) Optical image of a NNO-GDC-Ni/GDC microtubular cell; (c) Details of the electrolyte cracking of a cell sintered at 1200 °C.

2.2 Experimental Setup

Electrical connections were made using four platinum (Pt) wires. Pt mesh was used as current collector at the cathode side (inner side of the tube) and nickel paste (terpineol based) as current collector at the anode. The SOFC tube was sealed using Ceramabond 503 sealant (Aremco, US) into alumina extension tubes and this complete the arrangement introduced into a quartz tube, which was sealed again to separate both anode and cathode chambers. Additional details of the experimental setup can be found in [27]. The cell was heated to 750 °C in a small tubular furnace under pure oxygen (Q = 100 ml/min) at the cathode side and static air at the anode side. At this temperature, argon was introduced to purge the anode chamber for 10 minutes. Then humidified hydrogen (~3% H_2O) at 100 ml/min was introduced in order to reduce NiO into metallic Ni.

2.3 Electrochemical and Microstructural Characterization

Electrochemical measurements were carried out at temperatures between 750 °C and 600 °C. *j*–V (current density-voltage) and electrochemical impedance response measurements (EIS) were recorded using a VSP Potentiostat/Galvanostat (Princeton Applied Research, Oak Ridge, US). EIS were always recorded before and after each *j*–V measurement. SEM images before and after operation were obtained using a Merlin FE-SEM (Carl Zeiss, Germany).

3 Results and Discussion

3.1 Microstructure of the Cells

The microtubular cell dimensions are about 10 cm in length and the wall thickness of the NNO tube ca. 350 µm, as observed in Figure 1 (a). The GDC electrolyte and NiO-GDC anode layer appeared homogeneous from visual inspection as seen in Figure 1 (b), which was further confirmed in Figure 3b.

The microstructure of the cells is more closely observed in Figure 3 (SEM images were performed using a secondary electron detector). A homogeneous distribution of porosity was achieved in the NNO support consisting of pores of ~10 µm (produced by the pore former) and submicrometric pores formed during NNO-GDC co-sintering (Figure 3a). The multimodal porosity is also observed in Figure 3b together with a rather well bonded interface between the NNO cathode and GDC electrolyte phases. Reasonable adhesion was achieved between the electrolyte and both anode and cathode, as observed in Figures 3c. Cathode/electrolyte surface present a tree-root like interface, as both components are cosintered. As the anode is then deposited over the electrolyte and subsequently sintered at lower temperature, anode/electrolyte surface seems smoother. The same effect is observed for anode supported microtubular cells achieving good electrochemical performances and stable microstructures [11, 28]. Thicknesses of the GDC electrolyte were about 15 µm and the Ni-GDC anode was about 20 µm. It was expected that at the sintering temperature (1300 °C), the Si impurity reacts with Nd to form neodymium silicate ($Nd_4Si_3O_{12}$) [29]. In addition, decomposition of the A-site deficient phase into NiO and $Nd_2NiO_{4+\delta}$

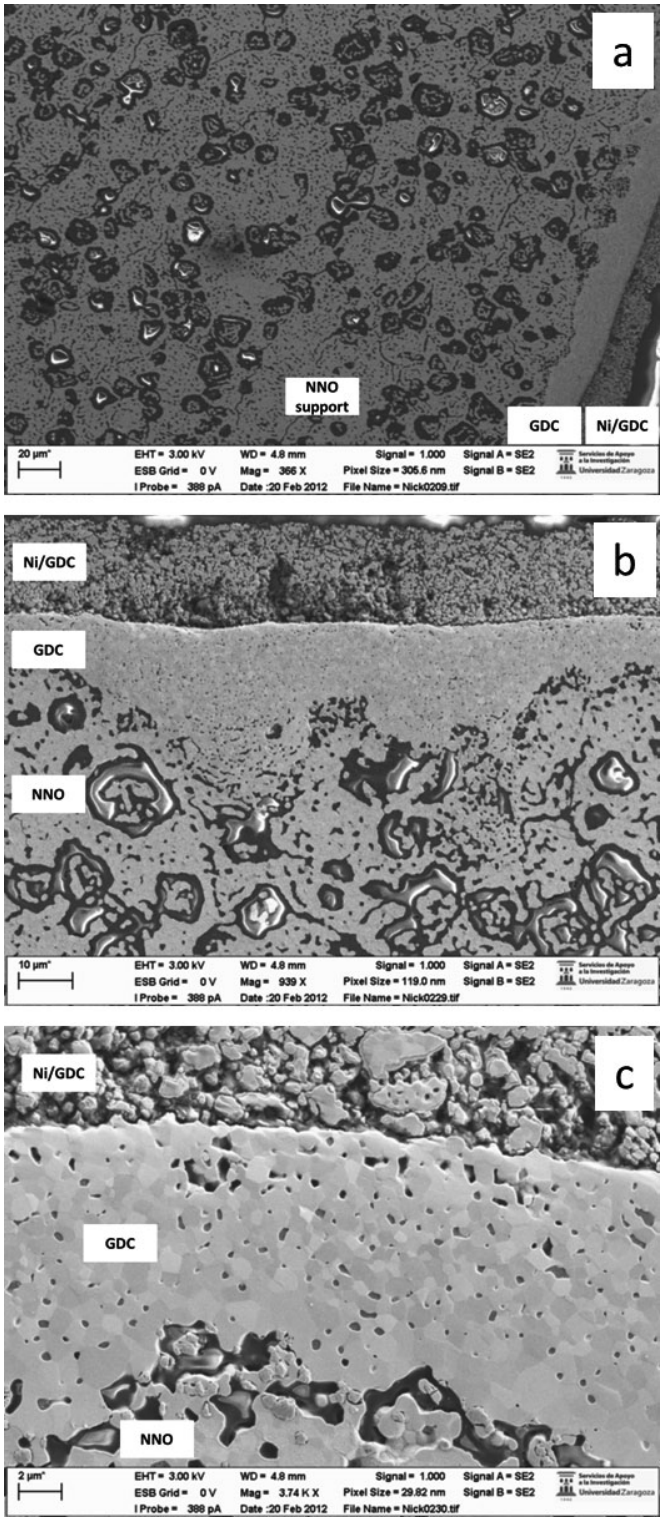

Fig. 3 Microstructure of the NNO-GDC-Ni/GDC microtubular cell showing (a) pore distribution at the NNO support; (b) microstructure of the GDC electrolyte; and (c) electrolyte-electrodes interfaces.

(reaction 1) occurred at 1300 °C and 1400 °C, as confirmed from the XRD patterns shown in Figure 4. As observed for those temperatures, and also previously reported by Schuler *et al.* [37], decomposition also takes place due to Si impurities in the raw NNO powder. Small amounts of silicon, introduced by milling during powder processing, reacts during sintering steps to form Nd-silicate phases decomposition, according to reaction 2 [25].

$$Nd_{1.95}NiO_{4+\delta} \rightarrow NiO + Nd_2NiO_{4+\delta} \quad (1)$$

$$Nd_{1.95}NiO_{4+\delta}.+ 0.03\ Si \rightarrow 0.01\ Nd_4Si_3O_{12} + 0.01\ Nd_2O_3 + 0.05\ NiO + 0.95\ Nd_2NiO_{4+\delta}. \quad (2)$$

Finally, the formation of a mixed neodymium-cerium oxide (of approximate composition $Nd_{0.4}Ce_{0.6}O_{1.8}$) was predicted at the typical sintering temperatures, according to reaction 3 [25].

$$Nd_{1.95}NiO_{4+\delta}.+ CeO_2 \rightarrow Nd_{0.4}Ce_{0.6}O_{1.8}+ NiO \quad (3)$$

Although we do not have evidence of the formation of this phase as we did not perform XRD studies after cosintering the cells, mixed Nd-Ce oxide phases might be present. From the best of our knowledge, those cubic mixed Nd-Ce oxide phases are vaguely reported in the literature and their conductivity is unknown. Possibly, they will perform as a MIEC (mixed ionic and electronic conductor), electronically due to the presence of Ce and also ionically conductive through oxygen vacancies. As a consequence, their presence should be beneficial for SOFC operation. Finally, EDX (Energy Dispersed X-Ray Spectrometry) analysis confirmed the presence of Si (supposedly as neodymium silicate), and nickel oxide precipitates were indeed observed at the NNO/GDC interface. Nonetheless, this rather strong reactivity at the presently used sintering temperature should not affect dramatically the electrical properties and performance of the cells. For instance, it was recently reported that some unreacted NiO and Nd_2O_3 in NNO composite cathodes, do not significantly affect the electrical performance of their cells [24].

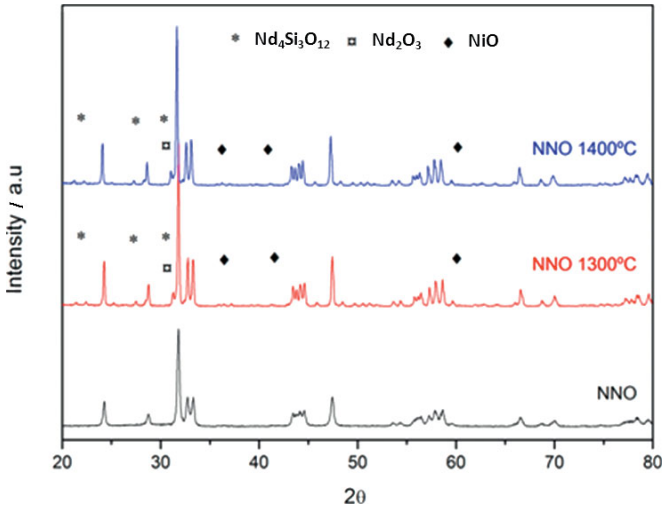

Fig. 4 XRD patterns showing the decomposition of the NNO phase: (a) NNO as received; (b) NNO sintered at 1300 °C for 2 hours; and (c) NNO sintered at 1400 °C for 2 hours.

3.2 Electrochemical Characterization

As displayed in Figure 5, the measured OCV values were 0.768 V, 0.753 V, 0.730 V and 0.696 V at 600 °C, 650 °C, 700 °C, and 750 °C, respectively. The obtained values are lower than those predicted form Nernst equation, attributable here to the internal short circuit current due to electrolyte reduction, as previously reported when using thin layers of ceria electrolyte [30]. To overcome this issue in the future, we are currently developing cells with a second electrolyte layer (based on ScSZ), acting as an electronic blocking layer to increase the OCV values towards their theoretical expectation.

From the *j*–V characteristics shown in Figure 5, peak power densities of 19, 25, 29 and 42 mW cm^{-2}, at 600, 650, 700 and 750 °C, respectively, were obtained. Although this performance is still lower in comparison with other cathode supported microtubular SOFC reported in the literature [15–18], in part due to a very high OCV loss, this is the first demonstration of electrochemical output with nickelates as cathode sup-

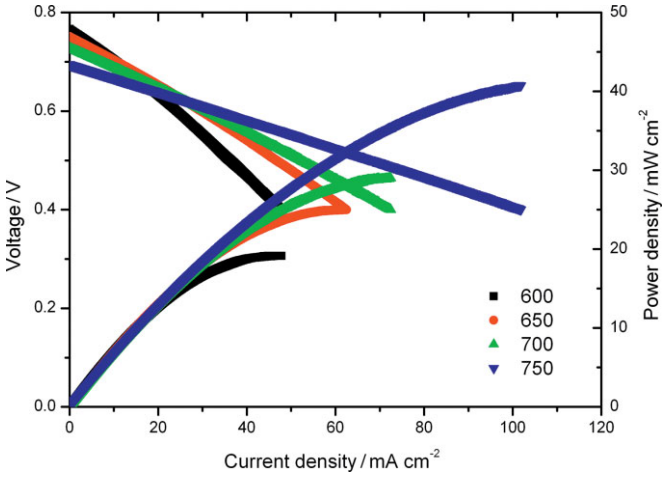

Fig. 5 *j*–V measurements for the NNO-GDC-Ni/GDC microtubular cell.

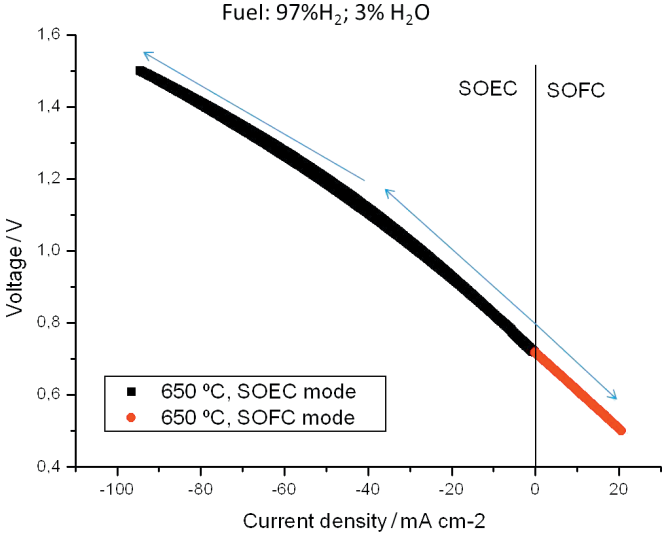

Fig. 6 *j*–V measurements (SOFC and SOEC) for the NNO-GDC-Ni/GDC microtubular cell at 650 °C.

ports for microtubular SOFC. On the other hand, as previously reported by Chauveau *et al.* [31], nickelates have shown better performance in solid oxide electrolysis cell (SOEC) mode than in SOFC mode, most likely due to the range of possible oxygen non-stoichiometries that the structure can adopt. We therefore performed preliminary SOEC studies using only 3% of steam at 650 °C (as shown in Figure 6). A change of slope is indeed observed under SOEC mode at current densities near –40 mA cm^{-2}, showing the potentiality of these cells for high temperature electrolysis applications. A similar effect was observed for the $La_{1.7}Sr_{0.3}Co_{0.5}Ni_{0.5}O_{4+\delta}$ (LSCN) oxygen electrode [32]. Complete characterization of improved cells under SOEC mode is currently carried out.

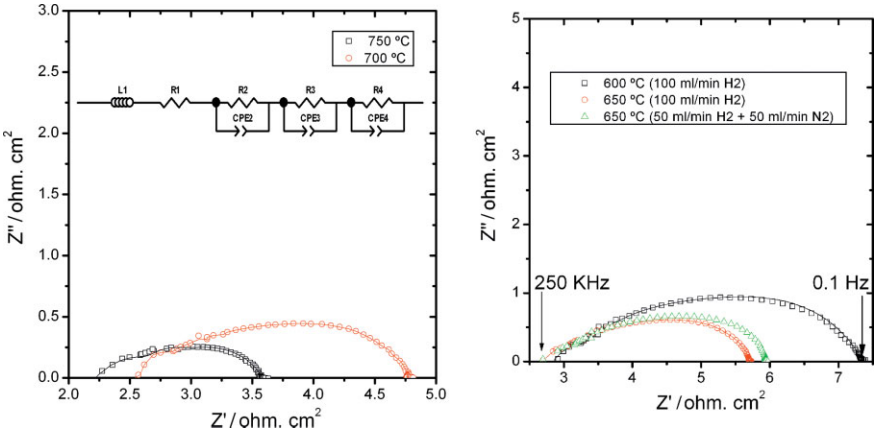

Fig. 7 AC impedance recorded prior to the *j*-V measurements for the NNO-GDC-Ni/GDC microtubular cell showing (symbols) experimental data and (solid line) fitting by the equivalent circuit presented in the inset.

AC impedance responses were registered prior and after each *j*–V curve as a function of temperature. In Figure 7, Nyquist plots recorded at OCV, before SOFC current load, are shown. An equivalent electrical circuit using the model also shown in Figure 7 was fitted to the experimental data. A summary of these results is given in Table 1. As expected, both ohmic and electrode polarizations are thermally activated. Ohmic resistances are by far higher than those expected for a GDC electrolyte layer of ~15 µm. Extra ohmic losses could be related with the previously described reactivities within the NNO and at the NNO-GDC interface, but more likely associated with lateral current collection losses along the NNO support, as electronic conduction of the NNO could be insufficient (an additional layer of Pt or Au will improve current collection). In addition, electrode polarization is in general large, especially at the lower temperatures (4.48 Ω cm^2 at 600 °C), while at higher temperatures (750 °C) the combined polarization of both electrodes is significantly reduced to 1.33 Ω cm^2. Based on previous studies in the literature [23, 32–37], it was attempted to assign the different contributions from the impedance response fitting to various limiting processes. For the studied temperature range, the high frequency (HF) contribution (R2, CPE2 component) arises at around 10 kHz and the capacitance values are in the range of ~10^{-6} Fcm^{-2}. In addition, R2 values show rather low temperature dependence (Table 1). Studies as a function of pH_2 confirmed that the HF contribution corresponds to the Ni/GDC anode, as this component increases when decreasing pH_2. In Ni/GDC cermets, the major rate limiting step is usually hydrogen adsorption and/or dissociation at the electrode surface, and those processes take place at frequencies under 100 Hz [33]. However, as this is not the case for our cells, the HF contribution could be associated with charge transfer at the anode, also based on the studies of Holtappels *et al.* [34], where the authors claim that at temperatures below 845 °C the impedance contribution for the Ni-YSZ anode was charge-transfer controlled. Although GDC is being used as ionic conductor in our case, the observed high HF contribution is indicating that our electrode present limited number of three-phase boundaries (TPBs) due to poor nickel dispersion in the YSZ matrix [35], and thus a charge-transfer limitation is suggested. This result is consistent with the high porosity observed in Figure 8 for the Ni/GDC anode, possibly due a poor sintering of the electrode. According to previous findings from Mauvy *et al.* [36], the medium frequency (MF)

Table 1 Resistances obtained by fitting the experimental EIS data for the NNO-GDC-Ni/GDC microtubular cell

Temperature (°C)	R1 (Ω cm^2)	R2 (HF) (Ω cm^2)	R3 (MF) (Ω cm^2)	R4 (LF) (Ω cm^2)	ASR_{total} (Ω cm^2)
600 before	2.86(3)	0.87(2)	1.83(4)	1.78(3)	7.34
600 after	2.86(2)	0.86(3)	1.76(5)	2.15(3)	7.63
650 before	2.70(2)	0.48(4)	1.01(2)	1.63(2)	5.82
650 (low pH_2)	2.70(3)	0.62(5)	1.03(4)	1.64(3)	5.99
650 after	2.70(2)	0.48(3)	1.09(2)	1.78(2)	6.05
700 before	2.48 (3)	0.29(2)	0.83(3)	1.18(2)	4.78
700 after	2.54(4)	0.30(2)	0.88(3)	1.27(2)	4.99
750 before	2.24(3)	0.33(2)	0.41(2)	0.59(3)	3.57
750 after	2.26(2)	0.35(2)	0.45(1)	0.66(2)	3.72

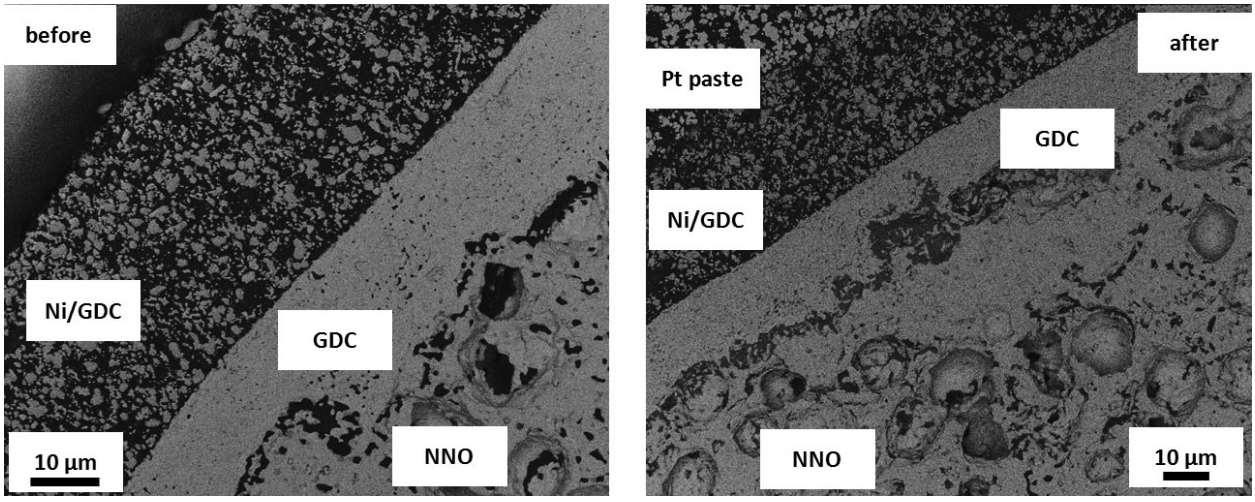

Fig. 8 SEM micrograph of the NNO-GDC-Ni/GDC microtubular cell before (left) and after (right) polarization.

contribution (R3, CPE3 component) and the low frequency (LF) contribution (R4, CPE4 component) are related to the NNO cathode. The MF contribution appears at around 1 kHz and the capacitance values are in the range of $\sim 10^{-5}$ F cm^{-2} (almost unaltered with temperature), and was associated to a combination of charge transfer reaction occurring on the electrode/gas interface (oxygen reduction on the surface of the cathode), and gas diffusion through the cathode support. Finally, the LF contribution, appearing at around 200 Hz and with capacitance values in the range of $\sim 10^{-4}$ F cm^{-2} (almost unaltered with temperature), were tentatively associated to oxygen ions transferring through the electrolyte/electrode interface. Although similar findings and polarization resistance values were also reported by Schuler *et al.* [37] and Mesguich *et al.* [38], the present assignation is very tentative. Note that previous works from references [36–38] were performed using symmetrical planar cells, and our case corresponds to a real fuel cell system using a thick oxygen electrode in tubular geometry. Those results are also consistent with recent studies for microtubular cells using NNO based cathodes [24], also considering that those results reported in reference 23 correspond to anode supported cells and the present study refers to cathode supported configuration. For example, at 600 °C charge transfer contributions of both anode and cathode appears at similar frequencies and their resistance values are also rather similar. Finally, as seen from table 1, a noticeable degradation (ca. 4% increase for all temperatures) is taking place at the cell electrodes after polarization measurements (for example, at 750 °C the total ASR was increased from 3.57 to 3.72 Ω cm^2). This degradation appears associated to the cathode only (mainly attributed to the LF contribution as observed from Table 1), as there was no apparent change in both the ohmic contribution (R1) and anode contribution (R2). As a consequence, proper fabrication of the NNO-GDC interface is the main focus for further development.

3.3 Microstructural Analysis after Operation

In Figure 8, SEM images after operation of the cells are presented. A micrograph of the cell using similar SEM conditions is also shown for comparison. Note that in this case a backscattered electron detector was used. The Ni/GDC–GDC interface apparently did not suffered any change, whereas an increase in porosity at the NNO-GDC interface was clearly observed. In addition, the adjacent NNO grains seem to be more densified. These results are in concordance with the AC impedance experiments, where the HF contribution (associated to the Ni-GDC anode) remained almost unaltered, and the MF and especially LF contribution (associated to the NNO cathode) increased after polarization. Based on EIS and SEM analysis, cathode contributions (both oxygen reduction on the surface of the NNO cathode and oxygen transfer from the cathode to the electrolyte) are clearly limiting the polarization of the cell. This problem could be avoided by the addition of a dense compact interlayer of the same NNO material next to the GDC electrolyte, as reported by Rieu *et al.* for the analogue $La_2NiO_{4+\delta}$ cathode material [39]. Finally, the previously mentioned reactivity between the NNO and the GDC electrolyte could be avoided by replacing the GDC electrolyte for LSGM (lanthanum strontium gallate magnesite), as it was reported that there is no evidence of secondary phase formation on nickelate-LSGM mixtures over a period of 72 h at temperatures of up to 1000 °C [40]. All subsequent studies are focused on the microstructure development, especially at the cathode-electrolyte interface, in order to increase fuel cell performance.

4 Summary

Results on the fabrication and characterization of neodymium nickelate cathode supported SOFC were presented. Peak power densities were 19, 25, 29 and 42 mW cm^{-2}, at 600, 650, 700 and 750 °C, respectively. Low OCV values were due to electronic conduction of the thin GDC electrolyte. In addi-

tion, rather strong chemical reactivity between the NNO support and the GDC electrolyte was present. In spite of this and although the performance is lower than other results reported in the literature using different SOFC cathodes, we believe that nickelates are potential candidates as cathode supports for microtubular SOFC and SOEC, once the composition and sintering conditions are properly tuned. Further studies will be performed by using bilayer electrolytes (GDC-ScSZ) and LSGM electrolytes.

Acknowledgements

The authors thank grant MAT2009-14324-C02-01 and MAT2012-30763, financed by the Spanish Government (Ministerio de Ciencia e Innovación) and Feder program of the European Community, for funding the project. We also thank Prof. V. M. Orera for discussion. The use of Servicio General de Apoyo a la Investigación (SAI, University of Zaragoza) is finally acknowledged.

References

[1] K. S. Howe, G. J. Thompson, K. Kendall, *J. Power Sources* **2011**, *196*, 1677.
[2] T. Suzuki, Y. Funahashi, T. Yamaguchi, Y. Fujishiro, M. Awano, Development of Fabrication/Integration Technology for Micro Tubular SOFCs, in: *Micro Fuel Cells: principles and applications*, (Ed: T. S. Zhao), Elsevier **2009**.
[3] V. Lawlor, *J. Power Sources* **2013**, *240*, 421.
[4] K. Yashiro, N. Yamada, T. Kawada, J. Hong, A. Kaimai, Y. Nigara, J. Mizusaki, *Electrochemistry* **2002**, *70*, 958.
[5] K. Kendall, M. Palin, *J. Power Sources* **1998**, *71*, 268.
[6] M. A. Laguna-Bercero, R. Campana, A. Larrea, J. A. Kilner, V. M. Orera, *J. Electrochem. Soc.* **2010**, *6*, B852.
[7] M. A. Laguna-Bercero, *J. Power Sources* **2012**, *203*, 4.
[8] I. P. Kilbride, *J. Power Sources* **1996**, *61*, 167.
[9] Y. H. Du, N. M. Sammes, *J. Power Sources* **2004**, *136*, 66.
[10] P. Sarkar, L. Yamarte, H. S. Rho, L. Johanson, *Int. J. Appl. Ceram. Tech.* **2007**, *4*, 103.
[11] R. Campana, R. I. Merino, A. Larrea, I. Villarreal, V. M. Orera, *J. Power Sources* **2009**, *192*, 120.
[12] T. Suzuki, T. Yamaguchi, Y. Fujishiro, M. Awano, *J. Electrochem. Soc.* **2006**, *153*, A925.
[13] Y. W. Sin, K. Galloway, B. Roy, N. M. Sammes, J. H. Song, T. Suzuki, M. Awano, *Int. J. Hydrogen Energy* **2011**, *36*, 1882.
[14] S. Hashimoto, H. Nishino, Y. Liu, K. Asano, M. Mori, Y. Funahashi, Y. Fujishiro, *J. Power Sources* **2008**, *181*, 244.
[15] Y. Liu, S. I. Hashimoto, H. Nishino, K. Takei, M. Mori, T. Suzuki, Y. Funahashi, *J. Power Sources* **2007**, *174*, 95.
[16] C. H. Zhao, R. Z. Liu, S. R. Wang, Z. R. Wang, J. Q. Qian, T. L. Wen, *J. Power Sources* **2009**, *192*, 552.
[17] T. Yamaguchi, S. Shimizu, T. Suzuki, Y. Fujishiro, M. Awano, *Electrochem. Commun.* **2009**, *10*, 1381.
[18] T. Yamaguchi, S. Shimizu, T. Suzuki, Y. Fujishiro, M. Awano, *J. Electrochem. Soc.* **2008**, *155*, B423.
[19] A. Tarancón, M. Burriel, J. Santiso, S. J. Skinner, J. A. Kilner, *J. Mater. Chem.* **2010**, *20*, 3799.
[20] S. J. Skinner, J. A. Kilner, *Solid State Ion* **2000**, *135*, 709.
[21] J. M. Bassat, P. Odier, A. Villesuzanne, C. Marin, M. Pouchard, *Solid State Ion.* **2004**, *167*, 341.
[22] C. N. Munnings, S. J. Skinner, G. Amow, P. Whitfield, I. Davidson, *Solid State Ion.* **2005**, *176*, 1895.
[23] B. Philippeau, F. Mauvy, C. Mazataud, S. Fourcade, J.-C. Grenier, *Solid State Ion.* **2013**, *249–250*, 17.
[24] M. A. Laguna-Bercero, A. R. Hanifi, H. Monzón, J. Cunningham, T. H. Etsell, P. Sarkar, *J. Mater. Chem. A* **2014**, *2*, 9764.
[25] H. Lübbe, Micro-tubular solid oxide fuel cells with nickelate cathode-support, PhD Thesis, Lausanne, EPFL, **2012**. https://infoscience.epfl.ch/record/174682?ln=en
[26] H. Luebbe, J. Van herle, H. Hofmann, P. Bowen, U. Aschauer, A. Schuler, F. Snijkers, H.- J. Schindler, U. Vogt, C. Lalanne, *Solid State Ion.* **2009**, *180*, 11.
[27] M. A. Laguna-Bercero, R. Campana, A. Larrea, J. A. Kilner, V. M. Orera, *Fuel Cells* **2011**, *11*, 116.
[28] H. Monzón, M. A. Laguna-Bercero, A. Larrea, B. I. Arias, A. Várez, B. Levenfeld, *Int. J. Hydrogen Energy* **2014**, *39*, 5470.
[29] W. M. Harris, J. J. Lombardo, M. B. DeGostin, G. J. Nelson, H. Luebbe, J. A. Schuler, J. Van herle, J. C. Andrews, Y. Liu, P. Pianetta, Y.-C. K. Chen, J. Wang, W. K. S. Chiu, *Solid State Ion.* **2013**, *237*, 16.
[30] Y. Yamaguchi, T. Suzuki, S. Shimizu, Y. Fujishiro, M. Awano, *J. Membr. Sci.* **2007**, *300*, 45.
[31] F. Chauveau, J. Mougin, J. M. Bassat, F. Mauvy, J. C. Grenier, *J. Power Source* **2010**, *195*, 744.
[32] M. A. Laguna-Bercero, N. Kinadjan, R. Sayers, H. El Shinawi, C. Greaves, S. J. Skinner, *Fuel Cells* **2011**, *11*, 102.
[33] S. Primdahl, M. Mogensen, *Solid State Ion.* **2002**, *152–153*, 597.
[34] P. Holtappels, I. Vinke, L. D. Haart, U. Stimming, *J. Electrochem. Soc.* **1999**, *146*, 2976.
[35] W. Z. Zhu, S. C. Deevi, *Mater. Sci. Eng. A* **2003**, *36*, 2228.
[36] F. Mauvy, C. Lalanne, J. M. Bassat, J. C. Grenier, H. Zhao, L. Huo, P. Stevens, *J. Electrochem. Soc.* **2006**, 153, A1547.
[37] J. A. Schuler, H. Luebbe, A. Hessler-Wysser, J. Van herle, *J. Power Sources* **2012**, *212*, 223.
[38] D. Mesguich, J.-M. Bassat, C. Aymonier, A. Brüll, L. Dessemond, E. Djurado, *Electrochim. Acta* **2013**, *87*, 330.
[39] M. Rieu, R. Sayers, M. A. Laguna-Bercero, S. J. Skinner, P. Lenormand, F. Ansart, *J. Electrochem. Soc.* **2010**, *157*, B477.
[40] R. Sayers, J. Liu, B. Rustumji, S. J. Skinner, *Fuel Cells* **2008**, *8*, 338.

